International Journal of Thermal Sciences 48 (2009) 1279–1293

Contents lists available at ScienceDirect

International Journal of Thermal Sciences

www.elsevier.com/locate/ijts

Natural convection in a non-Darcy anisotropic porous cavity with a finite heat source at the bottom wall

D. Jaya Krishna [a], Tanmay Basak [b], Sarit K. Das [a,*]

[a] Heat Transfer and Thermal Power Laboratory, Department of Mechanical Engineering, Indian Institute of Technology Madras, Chennai 600 036, India
[b] Department of Chemical Engineering, Indian Institute of Technology Madras, Chennai 600 036, India

ARTICLE INFO

Article history:
Received 12 September 2007
Accepted 28 November 2008
Available online 6 January 2009

Keywords:
Natural convection
Generalized non-Darcy approach
Anisotropic porous medium
Finite heat source

ABSTRACT

The problem of natural convection with heat source located at the bottom surface of a cavity containing anisotropic porous medium is analyzed numerically by a generalized non-Darcy approach. Initially for a Darcy–Rayleigh number of $Ra_m = 1000$ the computations are carried out both in non-Darcy ($Ra = 10^5$; $Da = 10^{-2}$) and Darcy ($Ra = 10^9$; $Da = 10^{-6}$) regimes by varying the anisotropic properties of the porous medium. The properties considered for the study are permeability ratio (K^*), inclination of the principal axes (θ) and ratio of Forchheimer constants (F^*). Results are presented in terms of Isotherms, streamlines, maximum temperature and average Nusselt number to understand the flow physics. It is observed that the anisotropic properties have significant influence on the flow behavior and heat transfer. Further correlations for average Nusselt number and maximum temperature at the heat source surface for wide range of parameters ($10^7 \leqslant Ra \leqslant 10^8$, $10^{-5} \leqslant Da \leqslant 10^{-3}$, $0.2 \leqslant w \leqslant 0.8$, $0^\circ \leqslant \theta \leqslant 90^\circ$, $0.1 \leqslant K^* \leqslant 10$ and $1 \leqslant F^* \leqslant 100$) in non-Darcy regime are presented.

1. Introduction

Natural convection in fluid saturated anisotropic porous media has attracted many researchers because of its wide spectrum of applications in engineering and nature. Such applications include thermal insulation, certain biological materials, casting of metal matrix composites, flow in mushy region of a solidifying alloy and flow past heat exchanger tubes [1,2]. The problem of heat source located on the bottom surface of a porous layer finds applications in disposal of nuclear wastes, electronic circuits, geothermal areas which consists of troughs of volcanic debris contained by walls of non-fragmented ignimbrite [3,4]. Prasad et al. [5] numerically studied two-dimensional natural convection in a rectangular cavity with finite isothermal heat source centrally located at one vertical wall. Hsiao et al. [6] numerically studied steady natural convection in an inclined porous cavity with a discrete heat source on a wall. El-Khatib and Prasad [4] and Robillard et al. [7] studied natural convection from a heat source on the bottom surface of a porous layer. Kimura and Bejan [8] studied natural convection in a stably heated corner filled with fluid saturated porous medium. Degan and co-investigators [9–11] numerically investigated natural convection in fluid saturated porous medium which is assumed to be hydrodynamically anisotropic with its principal axes oriented in a direction that is oblique to gravity vector. Mamou et al. [12] demonstrated that, the orientation of principal axes and permeability ratio have significant influence on the stability of the system for an anisotropic porous medium heated from below by a constant heat flux. Recently, Degan et al. [3] investigated non-Darcy natural convection arising from line or point heat source in a hydrodynamically anisotropic porous medium. In their study the principal axes is oriented in a direction that is oblique to the gravity vector.

It is evident from literature that the natural convection with heat source embedded in an anisotropic porous media is limited to either Darcy's relation or its modified forms. However, the earlier studies [13–16] in isotropic porous medium with generalized non-Darcy model suggests that the parameters such as Rayleigh number (Ra), Darcy number (Da), Forchheimer constant (F) and porosity (ε) do have significant influence on flow behavior. Nakayama et al. [17] numerically studied fluid flow and heat transfer through an anisotropic porous medium and demonstrated the function of macroscopic flow angle on directional Forchheimer coefficient. Knupp and Lage [18] provided tensor formulation for permeability and Forchheimer coefficients in which the principal axes were aligned with a Cartesian system of coordinates. Till date, a comprehensive study on natural convection in presence of heat source in anisotropic porous medium with proposed correlations for average Nusselt number and maximum base temperature in the non-Darcy regime is yet to appear in the literature.

The present study is a first attempt to analyze natural convection inside a square cavity filled with porous medium which is assumed to be anisotropic both in permeability and Forchheimer co-

* Corresponding author. Tel.: +91 44 2257 4655; fax: +91 44 2257 4652.
E-mail address: skdas@iitm.ac.in (S.K. Das).

1290-0729/$ – see front matter © 2008 Published by Elsevier Masson SAS.
doi:10.1016/j.ijthermalsci.2008.11.022

Nomenclature

C	Forchheimer coefficient (Eqs. (8), (9) and (13))	m^{-1}
C^*	ratio of Forchheimer coefficients (Eq. (11))	
Cp	specific heat	$J\,kg^{-1}\,K^{-1}$
Da	Darcy number (Eq. (17))	
F	Forchheimer constant	
F^*	ratio of Forchheimer constants (Eq. (10))	
g	acceleration due to gravity	$m\,s^{-2}$
Gr	Grashof number ($=\frac{g\beta\Delta TL^3}{\nu_f^2}$)	
K	permeability	m^2
k	thermal conductivity	$W\,m^{-1}\,K^{-1}$
K^*	permeability ratio (Eq. (7))	
k^*	thermal conductivity ratio (Eq. (15))	
L	cavity width (characteristic dimension)	m
Nu	local Nusselt number (Eq. (24))	
$\overline{Nu}$	average Nusselt number (Eqs. (25) and (26))	
P	pressure	$N\,m^{-2}$
Pr	Prandtl number	
q''	heat flux at the source	$W\,m^{-2}$
Ra	Rayleigh number (Eq. (17))	
Ra_m	Darcy–Rayleigh number ($=Ra\,Da$)	
T	temperature/non-dimensional temperature	K
t	time	s
T_m	non-dimensional maximum source temperature	
T_{max}	non-dimensional maximum temperature for constant heat flux at side walls	
T_s	non-dimensional temperature at heat source surface	
u	volume averaged velocity in x-direction	$m\,s^{-1}$
v	volume averaged velocity in y-direction	$m\,s^{-1}$
$\|V\|$	magnitude of velocity vector ($=\sqrt{u^2+v^2}$)	$m\,s^{-1}$
w	non-dimensional length of heat source	
x, y	coordinate axis	

Greek symbols

ψ	stream function	
ζ	u, v or T variable	
ρ	density	$kg\,m^{-3}$
ν	kinematic viscosity	$m^2\,s^{-1}$
μ	viscosity of fluid	$N\,s\,m^{-2}$
α_x	thermal diffusivity ($=\frac{k_x}{(\rho C_p)_f}$)	$m^2\,s^{-1}$
β	coefficient of thermal expansion	K^{-1}
ε	porosity (void volume/total volume)	
θ	inclination of principal axes	degree
σ	ratio of heat capacities (Eq. (4))	

Subscripts

f	fluid
p	porous medium
so	solid matrix
h	hot
c	cold
1, 2	direction of principal axes

Superscripts

$'$	non-dimensional quantities
$=$	tensor
$*$	ratio of anisotropic properties
$n, n-1$	present and previous time step
$i, i-1$	present and previous mesh index

efficient. It may be noted that the anisotropy is employed based on various inclinations of principal axes oriented with respect to gravity vector. For Darcy–Rayleigh number of $Ra_m = 1000$ and $\varepsilon = 0.8$, the computations are carried out both in non-Darcy ($Ra = 10^5$; $Da = 10^{-2}$) and Darcy ($Ra = 10^9$; $Da = 10^{-6}$) regimes by varying the anisotropic properties of the porous medium. The main parameters for the study are permeability ratio ($K^* = 0.1$, 1 and 10), inclination of principal axes ($\theta = 0°$, 45° and 90°) and ratio of Forchheimer constants ($F^* = 1$ and 10). In addition, the following wide range of parameters such as Rayleigh number ($10^7 \leqslant Ra \leqslant 10^8$), length of heat source ($0.2 \leqslant w \leqslant 0.8$), Darcy number ($10^{-5} \leqslant Da \leqslant 10^{-3}$), permeability ratio ($0.1 \leqslant K^* \leqslant 10$), inclination of principal axes ($0° \leqslant \theta \leqslant 90°$) and ratio of Forchheimer constants ($1 \leqslant F^* \leqslant 100$) have been considered to obtain correlations for average Nusselt number and maximum source temperature (T_m).

The objectives of the present work are chosen (a) to study the influence of parameters such as Ra, Da, w, K^*, θ and F^* in Darcy and non-Darcy regimes on the average Nusselt number and maximum temperature at the heat source surface and (b) to obtain correlations for average Nusselt number and maximum temperature at the heat source surface in an anisotropic porous cavity with a finite heat source at the bottom wall, which is of practical importance.

2. Mathematical formulation

The physical model as shown in Fig. 1 consists of a square cavity $L \times L$ whose side walls are kept at a constant temperature T_c. The bottom wall contains a symmetrically placed embedded heat source with constant heat flux, q'' with length w. The remaining parts of the bottom wall and the entire upper wall are adiabatic. It is assumed that the solid matrix of the porous media which is saturated by a homogeneous incompressible fluid does not undergo deformation and is anisotropic in permeability (Eq. (6)) as well as in Forchheimer coefficient (Eq. (8)). The fluid is assumed to be in local thermal equilibrium with the solid matrix. The thermophysical properties of the fluid are considered to be constant except for the density in the buoyancy term. Generalized non-Darcy approach has been considered and the governing equations are solved us-

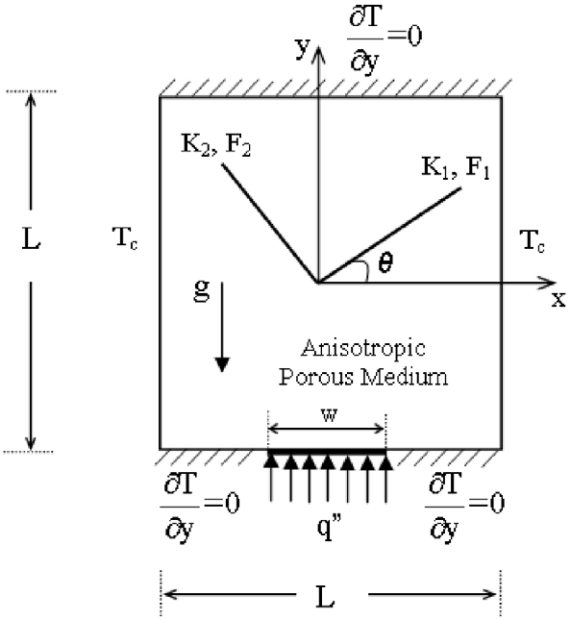

Fig. 1. Problem geometry.

ing a pseudo-transient approach. Hence, the equations in terms of primitive variables for transient flow can be written as follows

$$\nabla \cdot V = 0 \tag{1}$$

$$\frac{\rho_f}{\varepsilon}\left[\frac{\partial V}{\partial t} + \left(\frac{V}{\varepsilon}\right)\cdot\nabla V\right] = -\nabla P_f + \frac{\mu_f}{\varepsilon}\nabla^2 V - \frac{\mu_f}{\bar{\bar{K}}}V - \bar{\bar{C}}\rho_f V|V| + \rho_f \beta g(T - T_c) \tag{2}$$

$$(\rho Cp)_f\left[\frac{\partial(\sigma T)}{\partial t} + V\cdot\nabla T\right] = \nabla\cdot(\bar{\bar{k}}\nabla T) \tag{3}$$

where

$$\sigma = \frac{\varepsilon\rho_f Cp_f + (1-\varepsilon)\rho_{so}Cp_{so}}{\rho_f Cp_f} \tag{4}$$

$$k = \varepsilon k_f + (1-\varepsilon)k_{so} \tag{5}$$

$$\bar{\bar{K}} = \begin{bmatrix} K_1\cos^2\theta + K_2\sin^2\theta & (K_1-K_2)\sin\theta\cos\theta \\ (K_1-K_2)\sin\theta\cos\theta & K_2\cos^2\theta + K_1\sin^2\theta \end{bmatrix} \tag{6}$$

$$K^* = \frac{K_1}{K_2} \tag{7}$$

$$\bar{\bar{C}} = \begin{bmatrix} C_1\cos^2\theta + C_2\sin^2\theta & (C_1-C_2)\sin\theta\cos\theta \\ (C_1-C_2)\sin\theta\cos\theta & C_2\cos^2\theta + C_1\sin^2\theta \end{bmatrix} \tag{8}$$

$$C_1 = \frac{F_1}{\sqrt{K_1}}, \qquad C_2 = \frac{F_2}{\sqrt{K_2}} \tag{9}$$

$$F^* = \frac{F_1}{F_2} \quad \text{and} \tag{10}$$

$$C^* = \frac{C_1}{C_2} = \frac{F^*}{\sqrt{K^*}} \tag{11}$$

Substituting K^* (Eq. (7)) in Eq. (6) and by applying inverse, the permeability tensor can be reduced to

$$\overline{\overline{K^{-1}}} = \frac{1}{K_1}\begin{bmatrix} \cos^2\theta + K^*\sin^2\theta & (1-K^*)\sin\theta\cos\theta \\ (1-K^*)\sin\theta\cos\theta & K^*\cos^2\theta + \sin^2\theta \end{bmatrix} \tag{12}$$

Substituting C^* (Eq. (11)) in Eq. (8), the Forchheimer coefficient tensor can be reduced to

$$\bar{\bar{C}} = \frac{F_1}{\sqrt{K_1}}\begin{bmatrix} \cos^2\theta + \frac{\sqrt{K^*}}{F^*}\sin^2\theta & (1-\frac{\sqrt{K^*}}{F^*})\sin\theta\cos\theta \\ (1-\frac{\sqrt{K^*}}{F^*})\sin\theta\cos\theta & \frac{\sqrt{K^*}}{F^*}\cos^2\theta + \sin^2\theta \end{bmatrix} \tag{13}$$

$$\bar{\bar{k}} = \begin{bmatrix} k_x & 0 \\ 0 & k_y \end{bmatrix}, \tag{14}$$

$$k^* = \frac{k_y}{k_x} \tag{15}$$

Substituting k^* (Eq. (15)) in Eq. (14), the thermal conductivity tensor can be reduced to

$$\bar{\bar{k}} = k_x\begin{bmatrix} 1 & 0 \\ 0 & k^* \end{bmatrix} \tag{16}$$

The following non-dimensional parameters are employed

$$x' = \frac{x}{L}, \qquad y' = \frac{y}{L}, \qquad \alpha_x = \frac{k_x}{(\rho C_p)_f}$$

$$u' = u/(\alpha_x/L), \qquad v' = v/(\alpha_x/L), \qquad t' = t/(L^2/\alpha_x) \tag{17}$$

$$Pr = \frac{\nu_f}{\alpha_x}, \qquad Da = \frac{K_1}{L^2}, \qquad Ra = \frac{g\beta\Delta T L^3}{\nu_f\alpha_x}, \qquad P' = \frac{P_f}{(\rho\alpha_x^2/L^2)}$$

$$T' = \frac{T - T_c}{\Delta T}, \qquad \Delta T = \frac{q''L}{k_x}$$

For the sake of convenience prime symbol has been ignored and the governing equations in non-dimensional form are as follows:

$$\frac{\partial u}{\partial x} + \frac{\partial v}{\partial y} = 0 \tag{18}$$

$$\left[\frac{1}{\varepsilon}\frac{\partial u}{\partial t} + \frac{u}{\varepsilon^2}\frac{\partial u}{\partial x} + \frac{v}{\varepsilon^2}\frac{\partial u}{\partial y}\right] = -\frac{\partial P}{\partial x} + \frac{Pr}{\varepsilon}\left(\frac{\partial^2 u}{\partial x^2} + \frac{\partial^2 u}{\partial y^2}\right) - \frac{Pr}{Da}\left[u\left(\cos^2\theta + K^*\sin^2\theta\right) + v\left((1-K^*)\sin\theta\cos\theta\right)\right] - \frac{F_1}{\sqrt{Da}}\left[u\left(\cos^2\theta + \frac{\sqrt{K^*}}{F^*}\sin^2\theta\right) + v\left(\left(1 - \frac{\sqrt{K^*}}{F^*}\right)\sin\theta\cos\theta\right)\right]\sqrt{u^2+v^2} \tag{19}$$

$$\left[\frac{1}{\varepsilon}\frac{\partial v}{\partial t} + \frac{u}{\varepsilon^2}\frac{\partial v}{\partial x} + \frac{v}{\varepsilon^2}\frac{\partial v}{\partial y}\right] = -\frac{\partial P}{\partial y} + \frac{Pr}{\varepsilon}\left(\frac{\partial^2 v}{\partial x^2} + \frac{\partial^2 v}{\partial y^2}\right) - \frac{Pr}{Da}\left[u\left((1-K^*)\sin\theta\cos\theta\right) + v\left(K^*\cos^2\theta + \sin^2\theta\right)\right] - \frac{F_1}{\sqrt{Da}}\left[u\left(\left(1 - \frac{\sqrt{K^*}}{F^*}\right)\sin\theta\cos\theta\right) + v\left(\frac{\sqrt{K^*}}{F^*}\cos^2\theta + \sin^2\theta\right)\right]\sqrt{u^2+v^2} + Ra\cdot Pr\cdot T \tag{20}$$

$$\frac{\partial(\sigma T)}{\partial t} + u\frac{\partial T}{\partial x} + v\frac{\partial T}{\partial y} = \frac{\partial^2 T}{\partial x^2} + k^*\frac{\partial^2 T}{\partial y^2} \tag{21}$$

In the non-dimensional governing equations the Forchheimer constant is taken as $F_1 \approx 0.55$ which was experimentally measured by Ward [19] (also in [20]) and u and v are volume averaged components. The Prandtl number is taken to be 0.71 throughout the computations.

To check the validity of the present formulation and numerical procedure two different cases have been considered:

Case 1: Isothermally cooled side walls with finite heat source at the bottom wall.
Case 2: Constant heat flux at the side walls.

Initial and Boundary conditions are as follows (cases 1 and 2):

$$t = 0;\ u, v = 0,\ T = 0$$

Top wall

$$t > 0;\ u, v = 0,$$
$$\frac{\partial T}{\partial y} = 0 \quad \text{at } y = L;\ 0 \leqslant x \leqslant L$$

Bottom wall

Case 1

$$t > 0;\ u, v = 0,$$
$$\frac{\partial T}{\partial y} = 0 \qquad \text{at } y = 0;\ 0 < x \leqslant 0.5 - w/2$$
$$\frac{\partial T}{\partial y} = -1 \quad \text{at } y = 0;\ 0.5 - w/2 \leqslant x \leqslant 0.5 + w/2$$
$$\frac{\partial T}{\partial y} = 0 \qquad \text{at } y = 0;\ 0.5 + w/2 \leqslant x < L \tag{22}$$

Case 2

$t > 0;\ u, v = 0,$

$\dfrac{\partial T}{\partial y} = 0 \quad \text{at } y = 0;\ 0 < x \leqslant L$

Left wall

Case 1

$t > 0;\ u, v = 0,$

$T = 0 \quad \text{at } x = 0;\ 0 \leqslant y \leqslant L$

Case 2

$t > 0;\ u, v = 0,$

$\dfrac{\partial T}{\partial x} = -1 \quad \text{at } x = 0;\ 0 \leqslant y \leqslant L$

Right wall

Case 1

$t > 0;\ u, v = 0,$

$T = 0 \quad \text{at } x = L;\ 0 \leqslant y \leqslant L$

Case 2

$t > 0;\ u, v = 0,$

$\dfrac{\partial T}{\partial x} = -1 \quad \text{at } x = L;\ 0 \leqslant y \leqslant L$

The fluid motion has been displayed in terms of streamlines. The following relationships between the velocity components (u and v) and stream function (ψ) have been used

$$v = -\frac{\partial \psi}{\partial x}, \qquad u = \frac{\partial \psi}{\partial y} \tag{23}$$

The overall heat transfer rate is represented by average Nusselt number.

Case 1: The local Nusselt number at a given point on the heat source surface is defined by

$$Nu = \frac{1}{T_s(x)} \tag{24}$$

The average Nusselt number is defined by

$$\overline{Nu} = \frac{1}{w}\int_0^w \frac{1}{T_s(x)}\,dx \tag{25}$$

Case 2:

$$\overline{Nu} = \frac{1}{\Delta T} \tag{26}$$

Here, ΔT is the temperature difference between the mid height nodes at the vertical walls (Nithiarasu et al. [2]).

3. Numerical procedure

The governing equations have been discretized by using finite volume method. Quadrilateral cells in a semi-staggered arrangement introduced by Hirt et al. [21] have been employed. Velocity nodes are located at the vertices and pressure nodes are located at the centroid of the quadrilateral cells. First order upwind scheme is used for convective term formulation. Non-uniform grid has been employed.

For pressure and velocity coupling, the SIMPLE algorithm of Patankar [22] is used. The momentum equations are solved by Gauss–Seidel point by point iteration method. The iteration process is continued until the following convergence criterion is achieved.

$$\frac{\sum_{i,j} |\zeta_{i,j}^n - \zeta_{i,j}^{n-1}|}{\sum_{i,j} |\zeta_{i,j}^n|} < 10^{-8} \tag{27}$$

where ζ represents u, v or T variables.

4. Grid independence and validation

To validate the predictive capability and accuracy of the code, computations are performed with various configurations and boundary conditions. The simulation results are compared with the available literature [2,10,23] and the following strategies have been used.

Based on the definitions of porosity and Darcy number, as porosity tends to unity and Darcy number tends to infinity, the behavior of the porous media should tend towards single-phase fluid. For porosity being unity the total volume is identical with void volume. Darcy number, which is the non-dimensional form of permeability, can be stated as the ability of the solid matrix to allow the fluid to flow through it. If Darcy number tends to infinity, the ability of the fluid to flow through the solid matrix should tend to infinity, i.e. the restriction of the solid matrix should tend to zero. These concepts are useful to validate the codes for single phase fluid.

It may be noted that the simulations are based on non-uniform grid (uniform in x-direction, cosine in y-direction). To ensure the results obtained by the numerical study are independent of the computational grid, grid independence studies are carried out using Eq. (28) between two consecutive grids for maximum temperature. It is important to note that the number of iteration steps satisfying the convergence criteria increases with the increase in mesh size and this ensures a balance of convergence and computational time. It is found that the percentage deviation between 121×61 and 201×81 is less than 1%. Therefore a grid size of 121×61 is considered for simulation studies.

$$\%\text{Error} = \left(\frac{T_m^i - T_m^{i-1}}{T_m^i}\right) \cdot 100 \tag{28}$$

where T_m^i denotes maximum temperature for present grid size.

T_m^{i-1} denotes maximum temperature for previous grid size.

In order to check the validity of the present porous media code, the parameters $\varepsilon = 0.999$, $Da = 10^6$ and anisotropic properties, $\theta = 0°$, $K^* = 1$ and $F^* = 1$ are assumed as input. The simulation results are compared with the earlier work of Sharif and Mohammad [23] for natural convective flow in cavities with that of single phase fluid in presence of constant heat flux at the bottom wall and isothermal cooling from the side walls. The comparison between the present results with Sharif and Mohammad [23] is shown in Table 1.

Table 1
Comparison of present results for finite heat source with single phase fluid ($Da = 10^6$, $\varepsilon = 0.999$, $Pr = 1$, $\theta = 0°$, $K^* = 1$ and $F^* = 1$).

S. no.	Gr	w	$\overline{Nu}$ (Eq. (25))		T_m	
			Present	Sharif and Mohammad [23]	Present	Sharif and Mohammad [23]
1	10^3	0.2	5.745	5.926	0.1867	0.1819
2	10^5	0.6	5.731	5.864	0.2422	0.2432
3	10^5	0.8	5.761	5.864	0.2631	0.2651
4	10^4	0.4	4.082	4.132	0.2760	0.2745
5	10^6	0.6	9.691	9.949	0.1603	0.1631
6	10^6	0.2	11.060	11.341	0.1091	0.1092

Table 2
Comparison of present results for anisotropic porous medium ($Ra_m = 500$, $\varepsilon = 0.6$, $k^* = 1$ and $Pr = 1$).

S. no	Ra	Da	θ	K^*	$\overline{Nu}$ (Eq. (26))			T_{max}		
					Present code	Degan and Vasseur [10]	Nithiarasu et al. [2]	Present code	Degan and Vasseur [10]	Nithiarasu et al. [2]
1	5×10^7	10^{-5}	90	10^{-3}	5.652	5.909	5.660	0.241	0.247	0.248
2	5×10^5	10^{-3}	90	10^{-3}	4.489	4.727	4.560	0.295	0.305	0.305
3	5×10^7	10^{-5}	45	10^2	1.122	1.173	1.174	0.547	0.576	0.569
4	5×10^5	10^{-3}	45	10^2	1.121	1.170	1.170	0.547	0.576	0.570
5	5×10^7	10^{-5}	0	10^{-2}	9.452	10.781	9.950	0.245	0.261	0.236
6	5×10^5	10^{-3}	0	10^{-2}	5.064	5.414	4.729	0.293	0.304	0.314

The formulation for permeability tensor available in literature [2,10] has been considered assuming permeability K_1 inclined with angle θ to vertical axis. In the present study for the sake of convenience, the permeability tensor has been formulated assuming permeability K_1 with angle θ to horizontal axis (x-axis). Therefore, the angle 'θ' in the current study differs by 90° from the value reported by literature. For the validation of natural convective flow in anisotropic porous medium for wide range of permeability ratios, the case with constant heat flux boundary condition at the vertical side walls (case 2) has been considered and the results are compared with earlier works [2,10] by neglecting Forchheimer term and comparison is shown in Table 2. In summary, the rigorous tests of validation of computer code have been extensively carried out as shown in Tables 1 and 2. Finally, it may be remarked that, our test results agree well with the literature for both finite heat source and for anisotropic porous media.

5. Results and discussion

The following section demonstrates the influence of anisotropic properties such as permeability ratio (K^*), inclination of principal axes (θ) and ratio of Forchheimer constants (F^*) on the flow behavior and heat transfer. In this study, the permeability, K_1 is assumed to be constant, as Darcy number is defined in terms of K_1 and the permeability K_2 is varied with the change in K^* (Eqs. (7) and (17)). This section is based on two parts, the first part deals with the influence of anisotropic properties on the flow behavior and heat transfer within non-Darcy and Darcy regimes. In the second part the correlation for maximum temperature at the heat source surface in non-Darcy regime is obtained. The results are illustrated in terms of streamlines, isotherms, average Nusselt number and maximum temperature (T_m) on the heat source surface.

5.1. Comparison of non-Darcy and Darcy regimes

The anisotropic porous medium is provided with a symmetrically embedded heat source with constant heat flux which is 0.4 times of the length (L). The side walls are cooled with a constant temperature T_c and the remaining parts of the bottom wall and the entire upper wall are adiabatic. For a Darcy–Rayleigh number ($Ra_m = Ra \cdot Da$), $Ra_m = 1000$ and porosity of 0.8, the computations are carried out both in non-Darcy ($Ra = 10^5$, $Da = 10^{-2}$) and Darcy ($Ra = 10^9$, $Da = 10^{-6}$) regimes separately.

a) *Non-Darcy regime* ($Ra = 10^5$, $Da = 10^{-2}$)

i) *Effect of permeability ratio* (K^*): It is observed from Table 3 that with the increase in K^* for all θ and F^*, average Nusselt number decreases and maximum source temperature (T_m) increases. The illustration is carried out in terms of isotherms and streamlines as shown in Fig. 2 for $\theta = 45°$ and $F^* = 1$ with the variation of K^* from 0.1 to 10. It is interesting to observe that, vortex strength decreases with the increase in K^* and this is due to decrease in permeability in the direction of K_2. The variation of average Nusselt number and T_m is shown in Fig. 3 with K^*. A decreasing trend of average Nusselt number and increased trend of T_m is observed with the decrease in permeability in vertical direction. This is due to the fact that the decrease in permeability causes increase in obstruction for the flow field, which retards the flow and decreases convective transport. The decrease in convective strength leads to reduction of energy transport by which average Nusselt number decreases and T_m increases. The isotherm patterns as shown in Fig. 2 (a)–(c) illustrates that a gradual increase in magnitude of non-dimensional temperature at the heat source as K^* varies from 0.1 to 10.

Table 3
Influence of anisotropic properties in the non-Darcy flow regime ($Ra = 10^5$, $Da = 10^{-2}$, $\varepsilon = 0.8$, $Pr = 0.71$ and $w = 0.4$).

S. no.	θ	K^*	F^*	$\overline{Nu}$ (Eq. (25))	T_m	Location
1	0	0.1	1	5.629	0.2196	0.500, 0
2	0	1	1	5.188	0.2346	0.500, 0
3	0	10	1	4.296	(0.2707)	0.500, 0
4	45	0.1	1	5.457	0.2252	0.510, 0
5	45	1	1	5.188	0.2346	0.500, 0
6	45	10	1	4.423	0.2645	0.490, 0
7	90	0.1	1	5.310	0.2303	0.500, 0
8	90	1	1	5.188	0.2346	0.500, 0
9	90	10	1	4.609	0.2566	0.500, 0
10	0	0.1	10	5.747	(0.2160)	0.500, 0
11	0	1	10	5.374	0.2280	0.500, 0
12	0	10	10	4.319	0.2697	0.500, 0
13	45	0.1	10	5.514	0.2232	0.510, 0
14	45	1	10	5.299	0.2306	0.500, 0
15	45	10	10	4.459	0.2631	0.489, 0
16	90	0.1	10	5.329	0.2296	0.500, 0
17	90	1	10	5.236	0.2329	0.500, 0
18	90	10	10	4.651	0.2549	0.500, 0

ii) *Effect of inclination of principal axes* (θ): It is observed from Table 3 and Fig. 3 that the variation of the average Nusselt number and T_m, with K^* does not follow the systematic trend with the variation of θ. This is now explained as given below. It is observed from Fig. 3 that with $F^* = 1$ and for $K^* = 0.1$, the average Nusselt number decreases and T_m increases with the variation of θ from 0° to 90°. On the other hand for $K^* = 10$, the variation is observed in reverse manner. With $\theta = 0^0$ for $K^* = 0.1$, the permeability K_2 (i.e. vertical direction) is larger than that with K_1. As θ increases from 0° to 90° the permeability in vertical direction decreases and is 10 times less to that of the horizontal direction for $\theta = 90°$. The decrease in permeability in vertical direction causes increase in obstruction for flow which leads to decrease in average Nusselt number and increase in maximum source temperature for $K^* = 0.1$ with $\theta = 90°$. For $K^* = 10$, the increase in permeability in vertical direction with the increase in θ from 0° to 90° causes increase in average Nusselt number and decrease in T_m. Based on Eq. (10) with $F^* = 10$, it may be noted that the non-linear

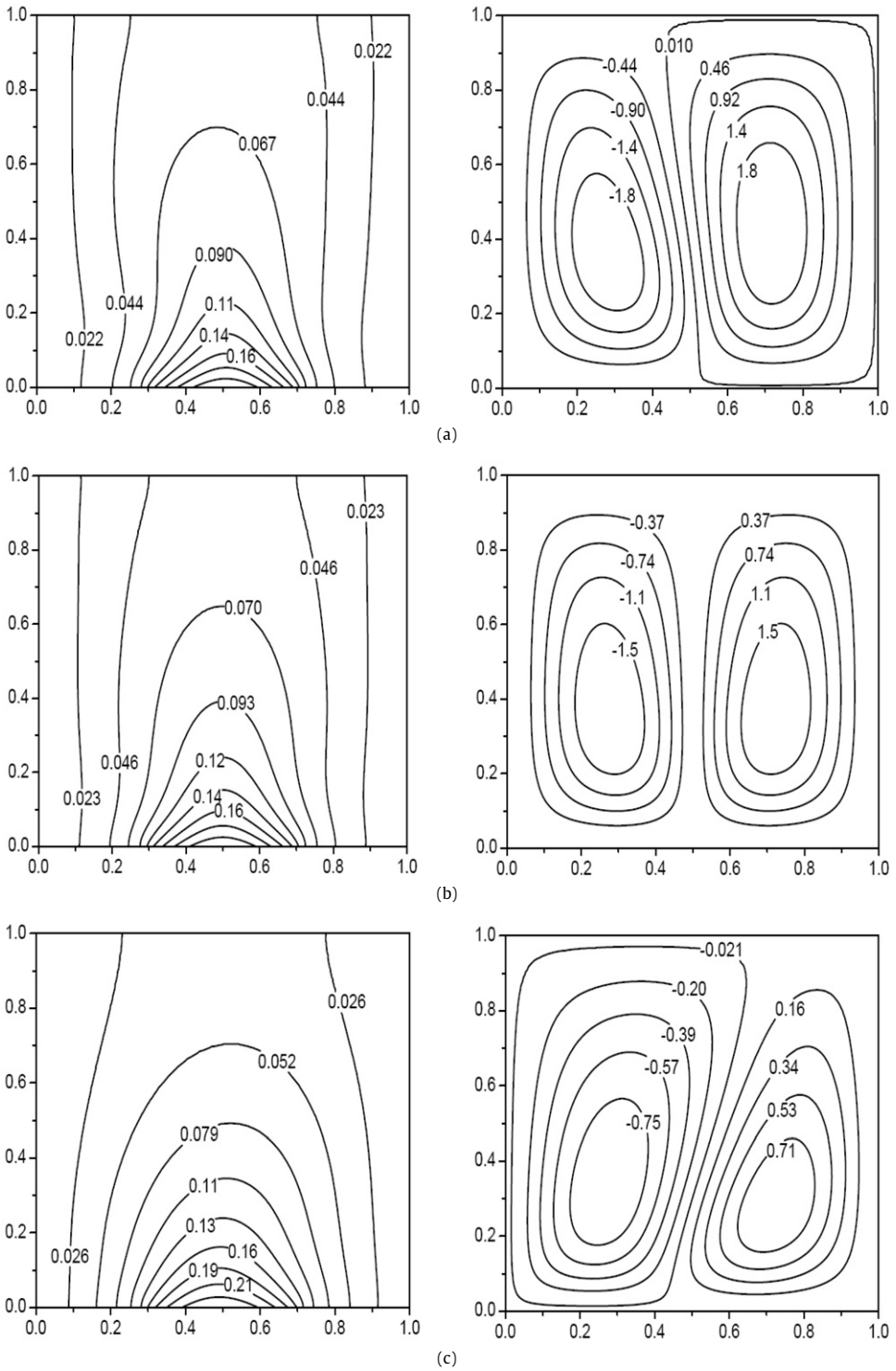

Fig. 2. Isotherms (left) and streamlines (right) in non-Darcy flow regime for $Ra = 10^5$, $Da = 10^{-2}$, $F^* = 1$, $\theta = 45°$ and $w = 0.4$. (a) $K^* = 0.1$ ($T_m = 0.225$); (b) $K^* = 1$ ($T_m = 0.235$); (c) $K^* = 10$ ($T_m = 0.264$).

drag is less in F_2 direction when compared to that of F_1. Fig. 4 illustrates isotherms and streamlines for $K^* = 0.1$ and $F^* = 10$ with the variation of θ from 0° to 90°. The highest permeability and lowest non-linear drag cause minimum obstruction for the flow field and result in higher vortex strength. Therefore, maximum vortex strength occurs for $K^* = 0.1$, $F^* = 10$ and $\theta = 0°$. As θ increases from 0° to 90°, the decrease in permeability and increase in non-linear drag in the direction of K_2 causes reduction in vortex strength. For $F^* = 10$, $K^* = 0.1$ and 1, the heat transfer rate decreases with the increase of θ. This is due to the fact that as θ increases, the intensity of circulation decreases. On the other hand, for $K^* = 10$ the increase in heat transfer rate is observed with the increase of θ. This is due to the fact that for $\theta = 0°$ with $F^* = 10$ the non-linear drag is lesser in vertical direction than that in horizontal direction. The increase in non-linear drag for $K^* = 1$ in vertical direction with the increase in θ causes increase in obstruction for flow field which leads to marginal decrease in heat trans-

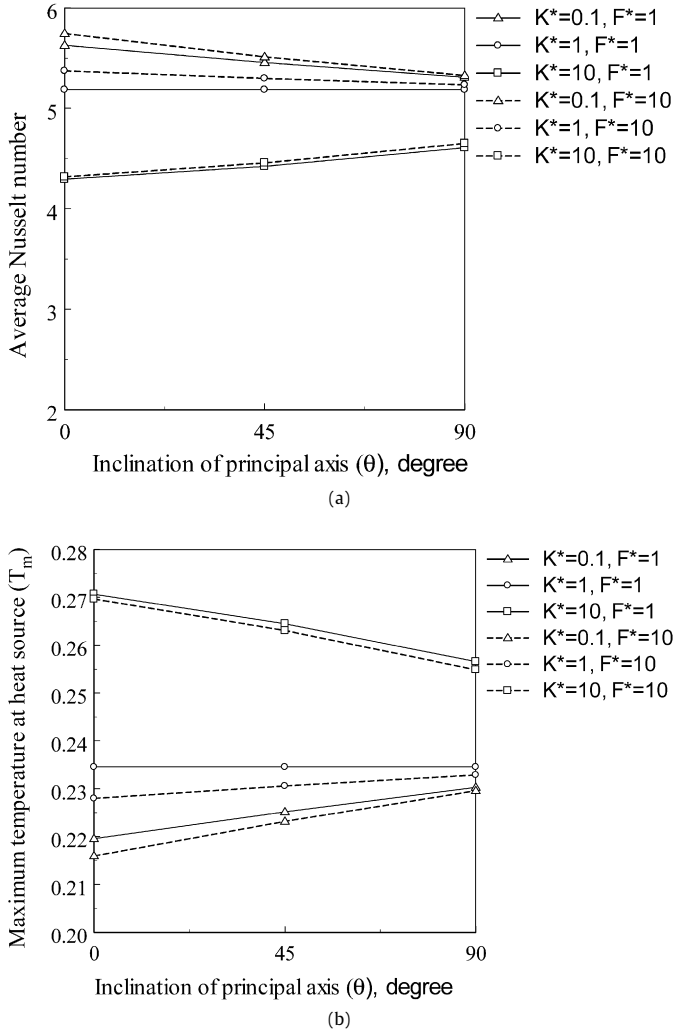

Fig. 3. Influence of K^*, F^* and θ in non-Darcy regime on (a) average Nusselt number, (b) maximum temperature (T_m).

fer. For $K^* = 0.1$, increase in non-linear drag and decrease in permeability with the increase in θ causes reduction in heat transfer rate. For $K^* = 10$, increase in heat transfer rate is observed with the increase in θ from 0° to 90° as permeability increases in vertical direction with the increase in θ.

iii) *Effect of ratio of Forchheimer constants* (F^*): It is observed from Table 3 and Fig. 3 that irrespective to the variation of K^* and θ with the increase in F^*, the average Nusselt number increases and T_m decreases marginally due to the reduction of non-linear drag. Due to the reduction of non-linear drag in F_2 direction with increase in F^*, there is a marginal increase in vortex strength which in turn leads to marginal enhancement of heat transfer. From Fig. 3 the difference in the values of average Nusselt number and T_m for $\theta = 0°$ with $K^* = 0.1$ and 1 is observed to be reduced with $K^* = 10$. The reduction in variation reflects that the effect of non-linear drag reduces with the decrease in permeability. For $Ra = 10^5$, $Da = 10^{-2}$ the influence of F^* can be considered to be insignificant as the variation in the values of average Nusselt number and T_m for $\theta = 0°$ with $K^* = 0.1$ is about 2%. As it is well understood that the increase in velocities of the flow field leads to the increase in non-linear drag. Evidently, the lower velocities of the buoyancy driven flows for $Ra = 10^5$, $Da = 10^{-2}$ result in the insignificant nature of F^*.

Table 4
Influence of anisotropic properties in the Darcy flow regime ($Ra = 10^9$, $Da = 10^{-6}$, $\varepsilon = 0.8$, $Pr = 0.71$ and $w = 0.4$).

S. no.	θ	K^*	F^*	$\overline{Nu}$ (Eq. (25))	T_m	Location
1	0	0.1	1	15.868	0.1029	0.500, 0
2	0	1	1	11.079	0.1466	0.500, 0
3	0	10	1	5.302	(0.2500)	0.500, 0
4	45	0.1	1	14.191	0.1105	0.560, 0
5	45	1	1	11.079	0.1466	0.500, 0
6	45	10	1	5.439	0.2349	0.470, 0
7	90	0.1	1	15.220	0.1167	0.500, 0
8	90	1	1	11.079	0.1466	0.500, 0
9	90	10	1	5.873	0.2226	0.500, 0
10	0	0.1	10	16.021	(0.1013)	0.500, 0
11	0	1	10	11.125	0.1461	0.500, 0
12	0	10	10	5.304	0.2499	0.500, 0
13	45	0.1	10	14.225	0.1097	0.569, 0
14	45	1	10	11.129	0.1461	0.500, 0
15	45	10	10	5.442	0.2349	0.470, 0
16	90	0.1	10	15.446	0.1156	0.500, 0
17	90	1	10	11.132	0.1462	0.500, 0
18	90	10	10	5.876	0.2225	0.500, 0

b) *Darcy regime* ($Ra = 10^9$, $Da = 10^{-6}$)

i) *Effect of permeability ratio* (K^*): It is observed from Table 4 and Fig. 5 that with the increase in K^*, for all θ and F^*, the average Nusselt number decreases and T_m increases. To analyze the influence of K^*, isotherms and streamlines are shown in Fig. 6 with the variation of K^* from 0.1 to 10 for $\theta = 45°$ and $F^* = 1$. Reduction of vortex strength and increase in magnitude of temperature field are observed with increase in K^*. The decrease in vortex strength is due to the decrease in permeability in the direction of K_2 as the obstruction for the flow field increases in vertical direction. The decrease in convective transport due to retardation of flow leads to the reduction of heat transfer rate and increase in T_m.

ii) *Effect of inclination of principal axes* (θ): It is observed from Table 4 and Fig. 5 that, the maximum source temperature (T_m) increases with θ for $K^* = 0.1$, whereas it decreases for $K^* = 10$ with the increase in θ. The decrease in average Nusselt number is observed with the increase in θ from 0° to 45°. On the other hand, increase in average Nusselt number is observed with the increase in θ from 45° to 90° for $K^* = 0.1$, but for $K^* = 10$ an increasing trend is followed. The physics for this irregular behavior is explained in terms of streamlines, isotherms, local Nusselt number and temperature distribution over the heat source. Fig. 7 illustrates streamlines and isotherms and Fig. 8 illustrates the local Nusselt number and temperature distribution at the heat source surface for $Ra = 10^9$, $Da = 10^{-6}$, $K^* = 0.1$ and $F^* = 10$ with the variation of θ from 0° to 90°. It is observed in Fig. 7 that for $K^* = 0.1$ as the anisotropic orientation angle increases from 0° to 90°, the convective strength of the flow field gradually decreases due to the reduction of permeability in vertical direction. The higher permeability for $\theta = 0°$ in vertical direction causes higher convective transport when compared to that of 45° and 90°. The asymmetric nature in isotherms, streamlines from Fig. 7 and local Nusselt number and temperature distribution is observed in Fig. 8 for $\theta = 45°$. The larger permeability at 45° inclinations causes the asymmetric nature. This is due to the fact that the strong left vortex leads to higher energy transport in left portion of the cavity and shifts the peak of the base temperature towards right. The higher energy transport in left portions of the cavity can be reflected from higher values of local Nusselt number in the left portion of the cavity. This causes the maximum base temperature to shift towards right (0.569, 0).

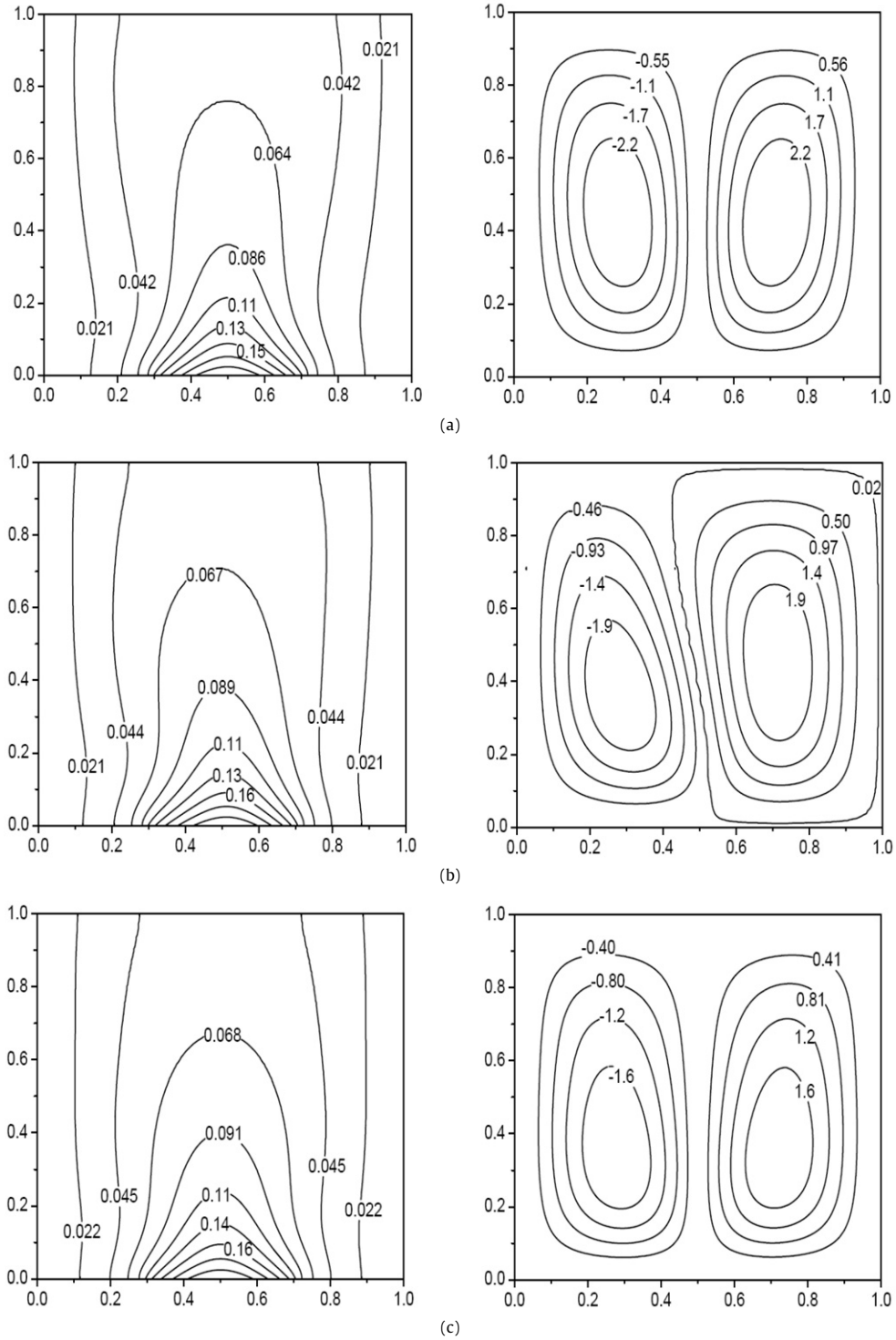

Fig. 4. Isotherms (left) and streamlines (right) in non-Darcy flow regime for $Ra = 10^5$, $Da = 10^{-2}$, $F^* = 10$, $K^* = 0.1$ and $w = 0.4$. (a) $\theta = 0^\circ$ ($T_m = 0.216$); (b) $\theta = 45^\circ$ ($T_m = 0.223$); (c) $\theta = 90^\circ$ ($T_m = 0.2296$).

For $\theta = 90^\circ$, the decrease in vortex strength and the movement of the vortices towards downward portion due to lower permeability causes increase in maximum base temperature and decrease in local Nusselt number. The decrease in average Nusselt number and increase in maximum base temperature for $\theta = 45^\circ$ can be explained in terms of temperature distribution and local Nusselt number over the heat source. Due to the weak right vortex which can be observed in Fig. 7(b) for $\theta = 45^\circ$ when compared to that of $\theta = 0^\circ$ (Fig. 7(a)) and $\theta = 90^\circ$ (Fig. 7(c)) the magnitude of local Nusselt number in the right half of the cavity is less. As a result the magnitude of the temperature distribution from $(0.569, 0)$ to $(0.7, 0)$ is more for $\theta = 45^\circ$ when compared to that of $\theta = 0^\circ$ and 90°. This can be referred for the uneven variation of average Nusselt number for $\theta = 45^\circ$. Increase in average Nusselt number and decrease in T_m is observed for $K^* = 10$. It may be noted that the permeability K_1 is assumed in terms of Darcy number and the permeability, K_2 is 10 times less compared to K_1

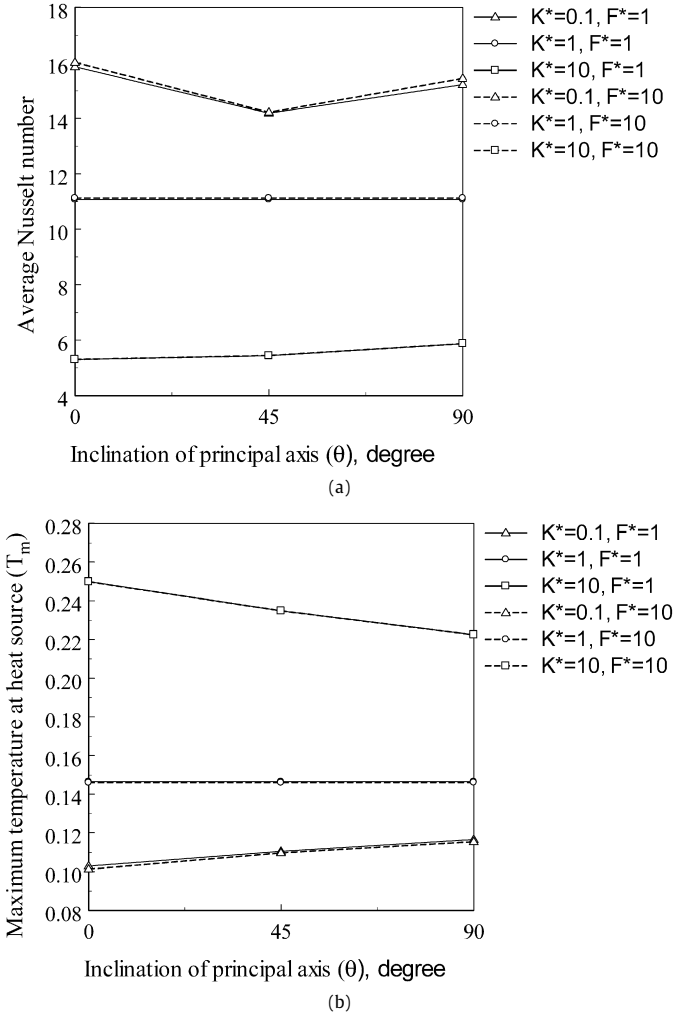

Fig. 5. Influence of K^*, F^* and θ in Darcy regime on (a) average Nusselt number, (b) maximum temperature (T_m).

for $K^* = 10$ and this results in vortex strength to be less for $\theta = 0°$. As θ increases, the permeability in vertical direction causes increase in vortex strength which in turn increases average Nusselt number and reduction in T_m. From Fig. 5 for $K^* = 1$, the influence of θ on F^* can be obtained. The insignificant nature of F^* reflects that in this regime the effect of non-linear drag is negligible.

iii) *Effect of ratio of Forchheimer constant* (F^*): It is observed from Fig. 5 that F^* is invariant with the variation of K^* and θ. This is due to the fact that the non-linear drag does not influence the flow behavior at lower permeabilities.

Based on the simulation results for $K^* = 10$, $\theta = 0°$ and $F^* = 1$, the linear and non-linear drags are maximum in vertical direction resulting in T_m to be maximum and average Nusselt number to be minimum. For $K^* = 0.1$, $\theta = 0°$ and $F^* = 10$, the linear and non-linear drags are minimum in vertical direction resulting in T_m to be minimum and average Nusselt number to be maximum. The increase in permeability and reduction in non-linear drag in vertical direction cause the reduction of obstruction for the flow in vertical direction and that result in increase in heat transfer and reduction in maximum source temperature.

Based on the parametric study, the non-Darcy and Darcy flow regimes are compared for a given Darcy–Rayleigh number ($= Ra \cdot Da$) and the observations are given below:

- For Darcy regime ($Da = 10^{-6}$), the large gradients are observed near to the heat source surface. This results in increased convective strength due to higher fluid velocities.
- In the Darcy regime, as the Rayleigh number is high for a fixed Darcy–Rayleigh number, the streamlines are dense. The larger gradients in temperature result in increase of average Nusselt number and decrease of maximum source temperature.
- In non-Darcy regime, larger convective mixing is found in the interior due to higher permeability.
- Based on Figs. 3 and 5 and the explanation carried out for F^*, the ratio of Forchheimer constants can be considered to be insignificant.

5.2. Correlation for T_m in non-Darcy regime

The range of parameters for the generation of correlation for maximum temperature (T_m) and average Nusselt number at the heat source surface in non-Darcy regime are $10^7 \leqslant Ra \leqslant 10^8$, $10^{-5} \leqslant Da \leqslant 10^{-3}$, $0.2 \leqslant w \leqslant 0.8$, $0° \leqslant \theta \leqslant 90°$, $0.1 \leqslant K^* \leqslant 10$ and $1 \leqslant F^* \leqslant 100$. In this section, along with the generation of correlation, the effects of *Ra*, *Da* and *w* on the flow behavior and heat transfer have been illustrated in terms of isotherms, streamlines and T_m.

i) *Effect of Rayleigh number* (*Ra*): The influence of *Ra* is shown in terms of isotherms and streamlines in Fig. 9 and in terms of local Nusselt number and temperature distribution on heat source in Fig. 10 for $Da = 10^{-3}$, $w = 0.4$, $K^* = 10$, $\theta = 45°$ and $F^* = 10$. It is observed in Fig. 9 that as Rayleigh number increases, the vortex strength also increases. It is observed in Fig. 10 that the peak of the temperature distribution along the heat source surface shifts towards left. This is due to the formation of strong right vortex as the permeability in the direction of K_2 is more. The weak left vortex results in lower energy transport in the left side of the cavity which can be observed from the variation of local Nusselt number. Due to higher vortex strength for $Ra = 10^8$ when compared to that of 10^7 the magnitude of temperature distribution for $Ra = 10^7$ is observed to be less. The increase in vortex strength leads to thinner velocity and thermal boundary layer and larger heat transfer rate resulting in reduction of T_m and increase in average Nusselt number.

ii) *Effect of Darcy number* (Da): Fig. 11 illustrates isotherm and streamline patterns for $Ra = 10^8$, $w = 0.4$, $K^* = 0.1$, $\theta = 90°$ and $F^* = 1$ with the variation of Darcy number from 10^{-3} to 10^{-5}. For a given set of parameters with the decrease in Darcy number, due to lower permeability of the medium, decrease in vortex strength can be observed. This leads to decrease in convective transport and as a result T_m increases.

iii) *Effect of heat source length* (w): The size effects of the heat source on the thermal and fluid fields are shown in Fig. 12 for $Ra = 10^8$, $Da = 10^{-4}$, $\theta = 0°$, $K^* = 1$ and $F^* = 1$ of w from 0.2 to 0.8. Fig. 12 (a) and (b) indicate that, the convection stratifies the temperature contours due to increase in heat source length and T_m increases with the increase in heat source length.

The influence of anisotropic properties has been already discussed in the comparison of Darcy and non-Darcy regimes.

Correlations for average Nusselt number and maximum temperature at the heat source (T_m) can be correlated in terms of Rayleigh number ($10^7 \leqslant Ra \leqslant 10^8$), Darcy number ($10^{-5} \leqslant Da \leqslant 10^{-3}$), length of the heat source ($0.2 \leqslant w \leqslant 0.8$), inclination of principal axes ($0° \leqslant \theta \leqslant 90°$), permeability ratio ($0.1 \leqslant K^* \leqslant 10$) and ratio of Forchheimer constants ($1 \leqslant F^* \leqslant 100$) as

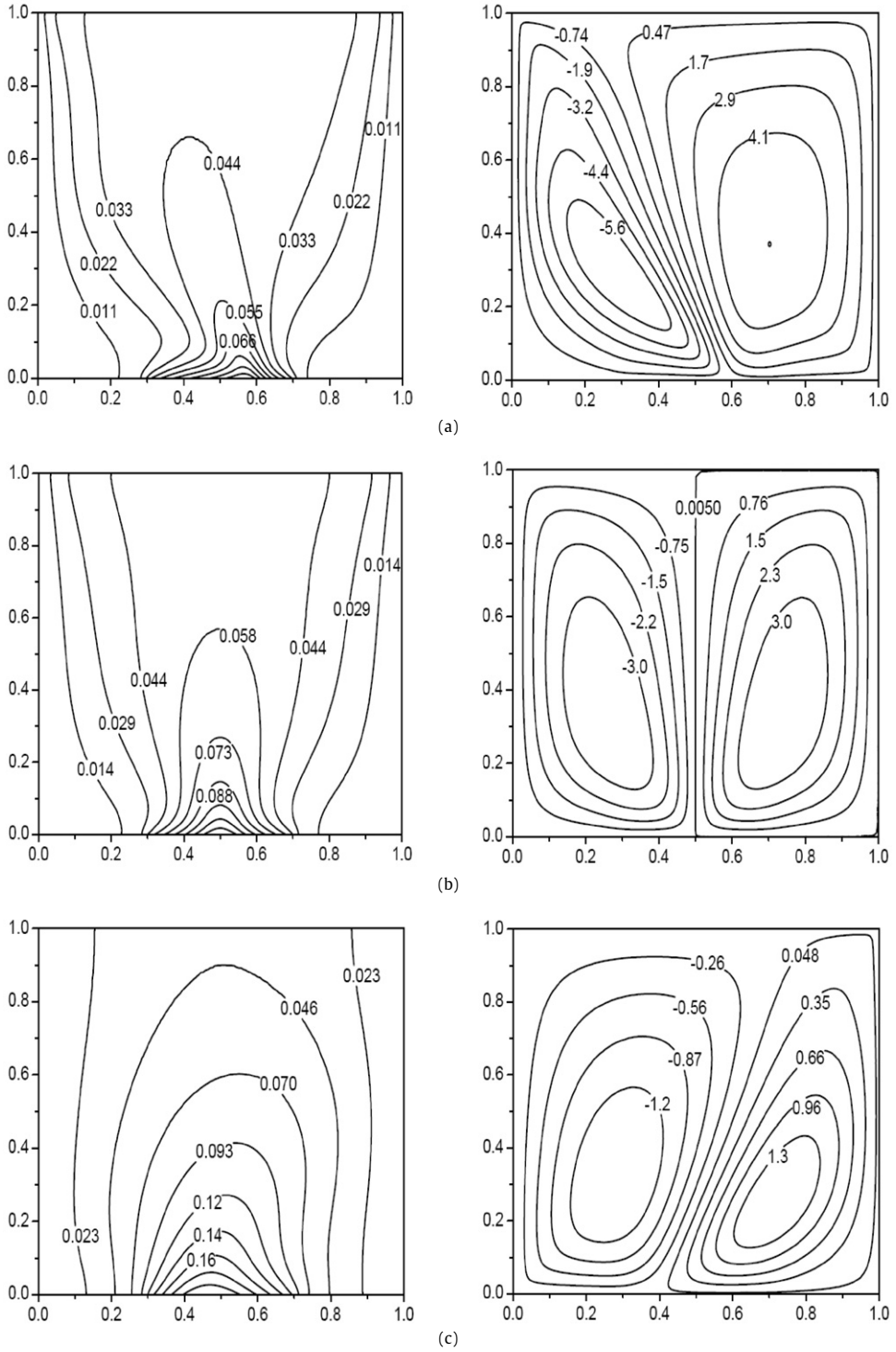

Fig. 6. Isotherms (left) and streamlines (right) in Darcy flow regime for $Ra = 10^9$, $Da = 10^{-6}$, $F^* = 1$, $\theta = 45°$ and $w = 0.4$. (a) $K^* = 0.1$ ($T_m = 0.1105$); (b) $K^* = 1$ ($T_m = 0.1466$); (c) $K^* = 10$ ($T_m = 0.2349$).

$$\overline{Nu} = 0.268Ra^{0.323}Da^{0.203}w^{-0.155}K^{*-0.086}(1+\sin\theta)^{-0.11}F^{*-0.0018} \tag{29}$$

$$T_m = 3.654Ra^{-0.271}Da^{-0.172}w^{0.3351}K^{*0.0769}(1+\sin\theta)^{0.07074} \times F^{*-0.0015} \tag{30}$$

Parity plots for average Nusselt number and T_m with an error band of ±10% is shown in Fig. 13. The average Nusselt number and maximum temperature at the heat source surface obtained by using the correlation compares with correlation coefficients of 0.917 and 0.978 to the values obtained by the numerical study. It may be noted that as the power of F^* is −0.0018 for average Nusselt number and −0.0015 for T_m the effect of F^* can be neglected for the considered range of parameters.

6. Conclusions

In the present study, the problem of heat source located on the bottom surface of an enclosure containing anisotropic porous

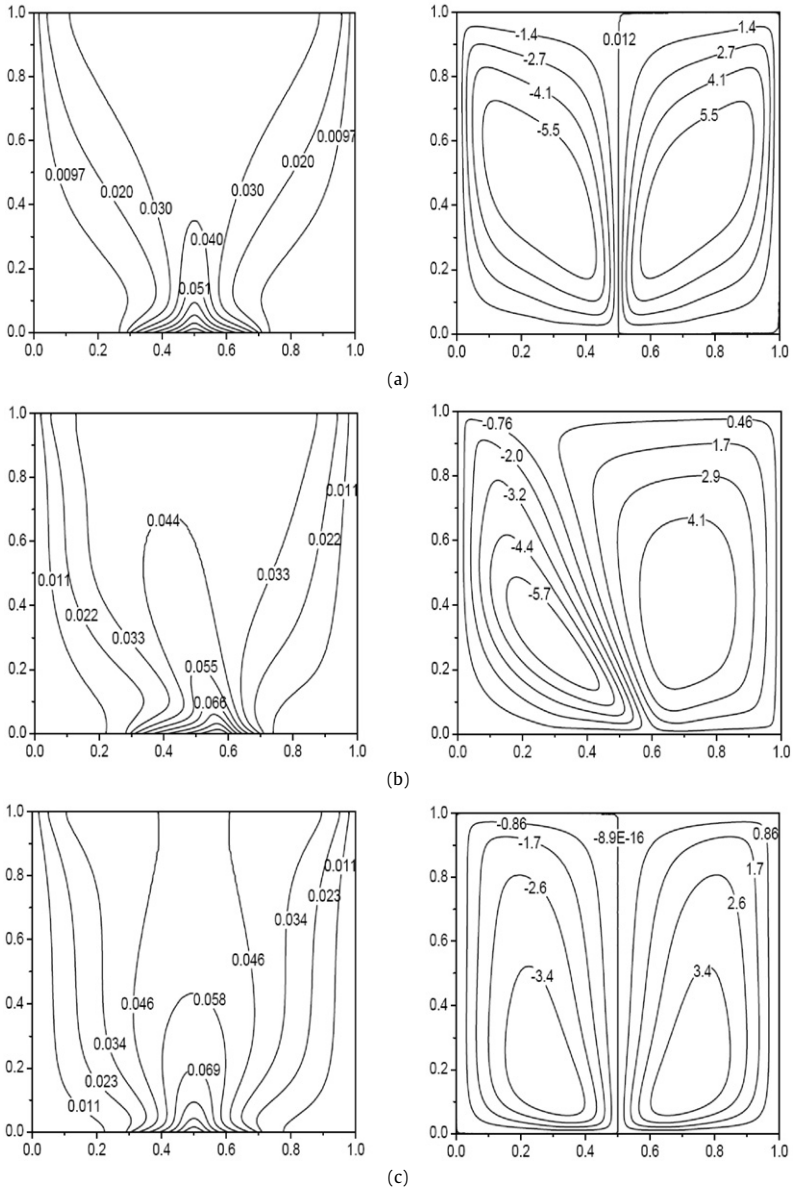

Fig. 7. Isotherms (left) and streamlines (right) in Darcy flow regime for $Ra = 10^9$, $Da = 10^{-6}$, $F^* = 10$, $K^* = 0.1$ and $w = 0.4$. (a) $\theta = 0^\circ$ ($T_m = 0.1013$); (b) $\theta = 45^\circ$ ($T_m = 0.1097$); (c) $\theta = 90^\circ$ ($T_m = 0.1156$).

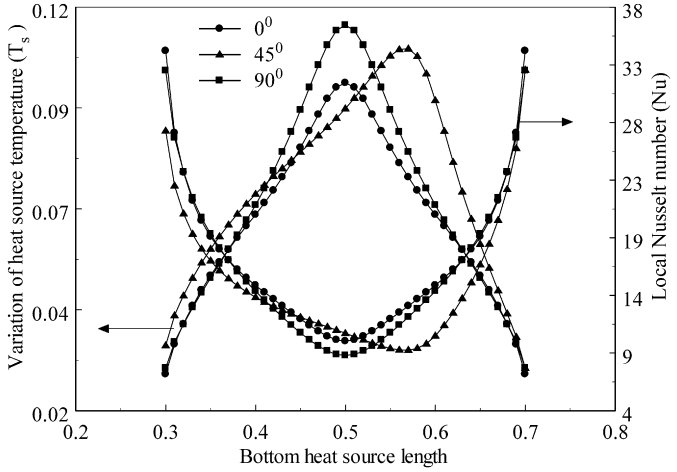

Fig. 8. Temperature distribution and local Nusselt number along the heat source surface for $Ra = 10^9$, $Da = 10^{-6}$, $w = 0.4$, $K^* = 0.1$ and $F^* = 10$ with θ.

medium is analyzed numerically by generalized non-Darcy approach. The present formulation is rigorously validated with the results available in literature. Initially, for a Darcy–Rayleigh number $Ra_m = 1000$, the computations are carried out both in non-Darcy ($Ra = 10^5$; $Da = 10^{-2}$) and Darcy ($Ra = 10^9$; $Da = 10^{-6}$) regimes by varying the anisotropic properties of the porous medium. The properties considered are permeability ratio (K^*), inclination of principal axes (θ) and ratio of Forchheimer constants (F^*). The effect of each parameter on the flow and the temperature fields are demonstrated in terms of isotherms, streamlines, average Nusselt number and maximum temperature at the heat source in order to explain the physics of fluid and thermal transport in the chosen geometry.

Subsequently, correlations for average Nusselt number and maximum temperature at the heat source surface in non-Darcy regime ($10^7 \leqslant Ra \leqslant 10^8$, $10^{-5} \leqslant Da \leqslant 10^{-3}$, $0.2 \leqslant w \leqslant 0.8$, $0^\circ \leqslant \theta \leqslant 90^\circ$, $0.1 \leqslant K^* \leqslant 10$ and $1 \leqslant F^* \leqslant 100$) have been developed.

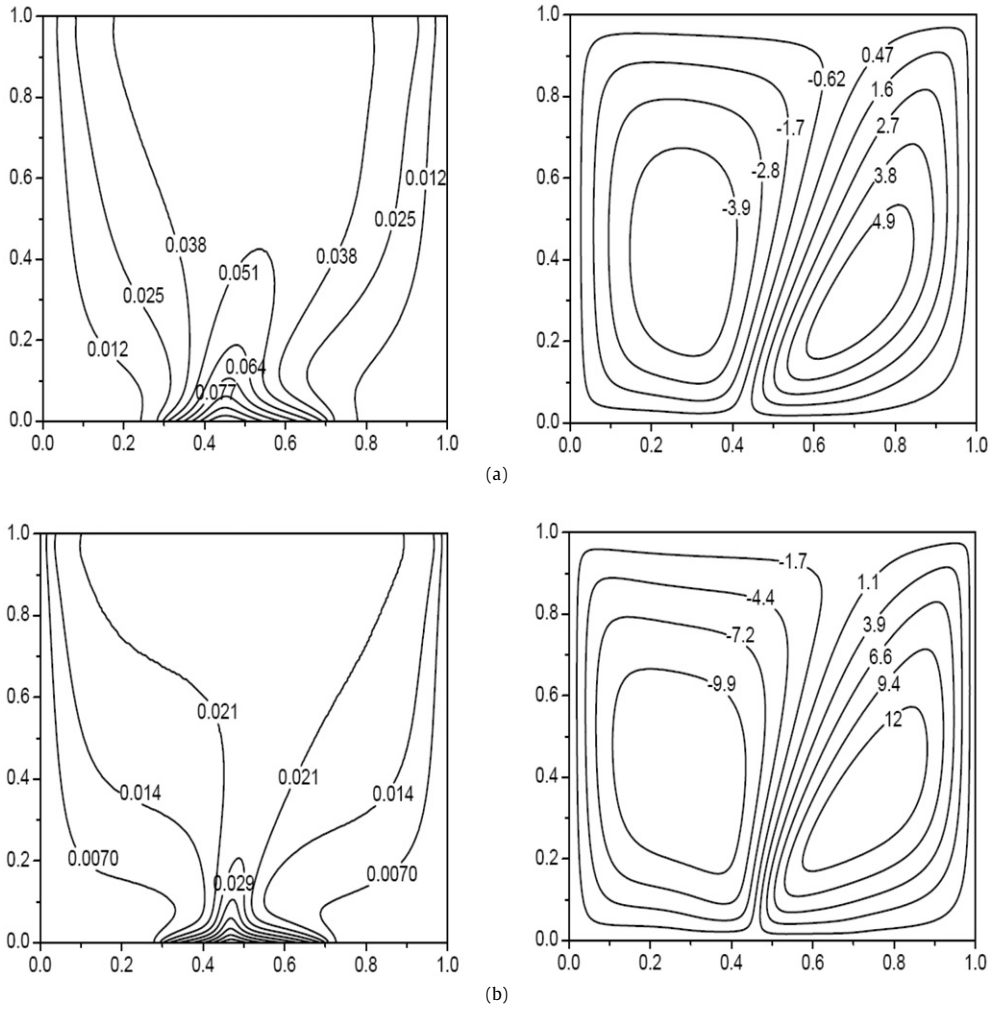

Fig. 9. Isotherms (left) and streamlines (right) with the variation of Rayleigh number in non-Darcy flow regime for $Da = 10^{-3}$, $\theta = 45°$, $w = 0.4$, $K^* = 10$ and $F^* = 10$. (a) $Ra = 10^7$ ($T_m = 0.1288$); (b) $Ra = 10^8$ ($T_m = 0.0717$).

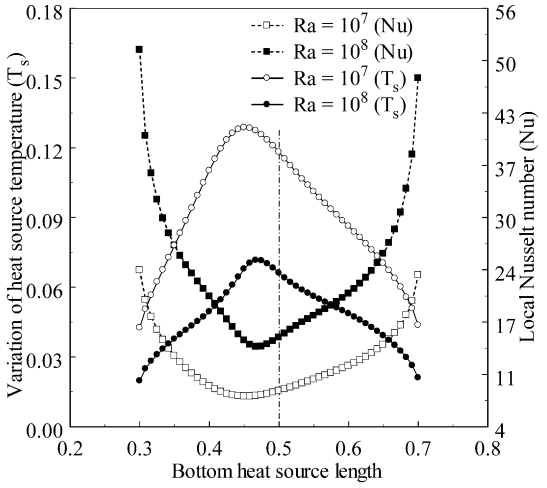

Fig. 10. Influence of Rayleigh number on the local Nusselt number and temperature distribution along the heat source surface for $Da = 10^{-3}$, $w = 0.4$, $K^* = 10$, $\theta = 45°$ and $F^* = 10$.

Based on the parametric study, the following conclusive remarks have been obtained:

- The velocity and the temperature gradients close to the heat source surface are enhanced in the Darcy regime due to increase in Rayleigh number.
- In the non-Darcy regime, convective mixing occurs in the interior region due to higher permeability whereas in Darcy regime the convective mixing occurs in the lower portions of the cavity due to lower permeability.
- Increase in convective strength due to higher fluid velocity close to the heat source surface in Darcy regime ($Da = 10^{-6}$) results in reduction of maximum base temperature compared to non-Darcy regime.
- For $\theta = 0°$ with $K^* = 0.1$ and $F^* = 10$, maximum enhancement in heat transfer is observed. The higher permeability and lower non-linear drag in vertical direction cause higher mobility of the fluid and increase energy transport.
- The lower velocities of the buoyancy driven flows for the considered parameters result in the insignificant nature of F^*. From Figs. 3, 5 and exponent of F^* in Eqs. (29) and (30) it may be observed that influence of F^* is insignificant.
- With the increase of Rayleigh number, increase in vortex strength is observed. The increase in vortex strength leads to thinner velocity and thermal boundary layer resulting in enhancement of heat transfer by which T_m is reduced.

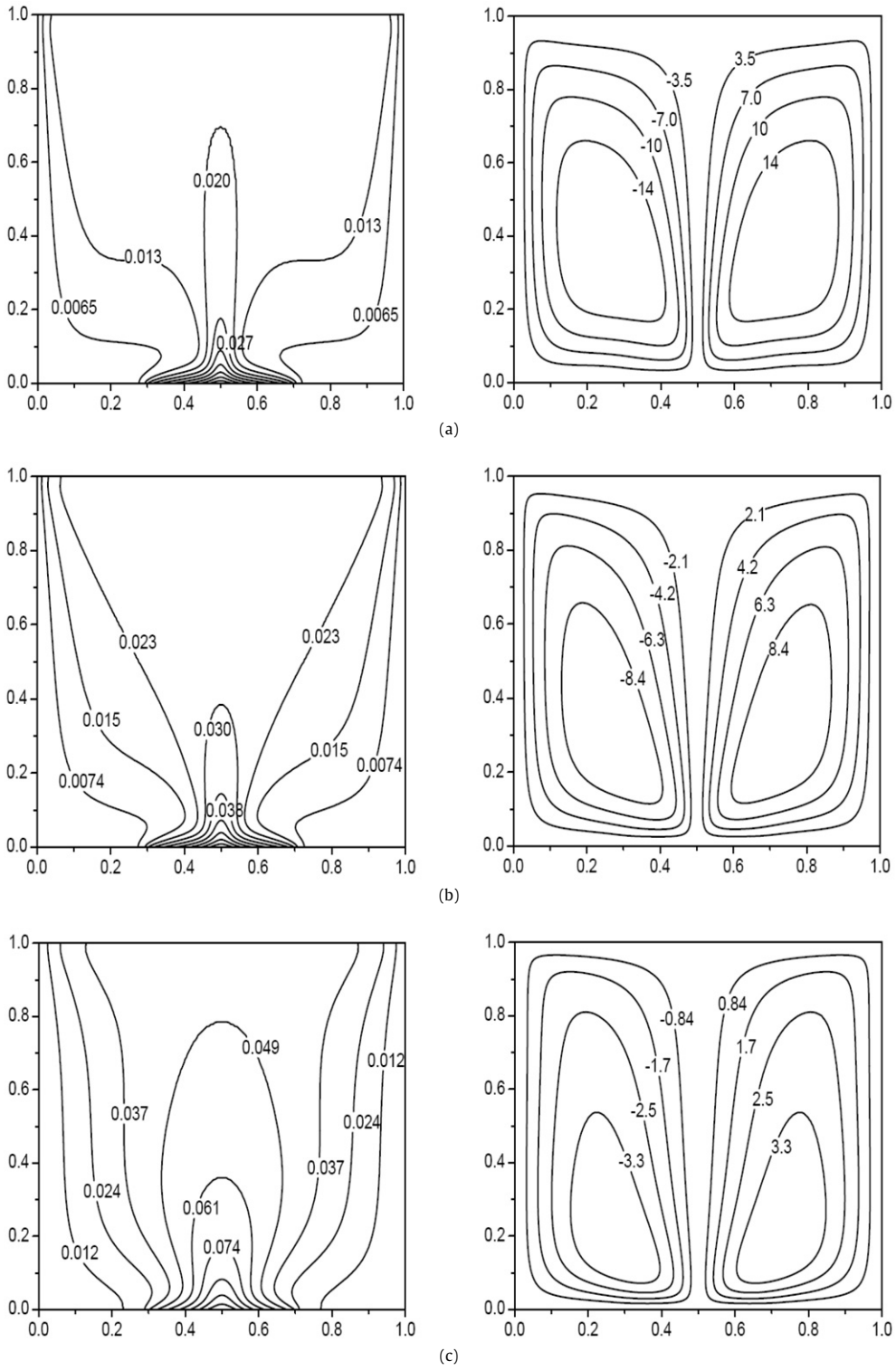

Fig. 11. Isotherms (left) and streamlines (right) with the variation of Darcy number in non-Darcy flow regime for $Ra = 10^8$, $K^* = 0.1$, $\theta = 90°$, $F^* = 1$ and $w = 0.4$. (a) $Da = 10^{-3}$ ($T_m = 0.0604$); (b) $Da = 10^{-4}$ ($T_m = 0.0761$); (c) $Da = 10^{-5}$ ($T_m = 0.1233$).

- Larger flow velocity is observed with the increase in Darcy number (permeability). The increase in convective transport due to larger flow velocity increases energy transport and therefore T_m is reduced.
- It is observed that T_m gradually increases due to the stratification of temperature contours with the increase in heat source length.
- Correlations for average Nusselt number and maximum temperature at the heat source are developed using regression analysis for wide range of parameters. The correlations developed are found to compare well with the average Nusselt number and maximum temperature based on numerical solutions with correlation coefficients of 0.917 and 0.978 respectively.

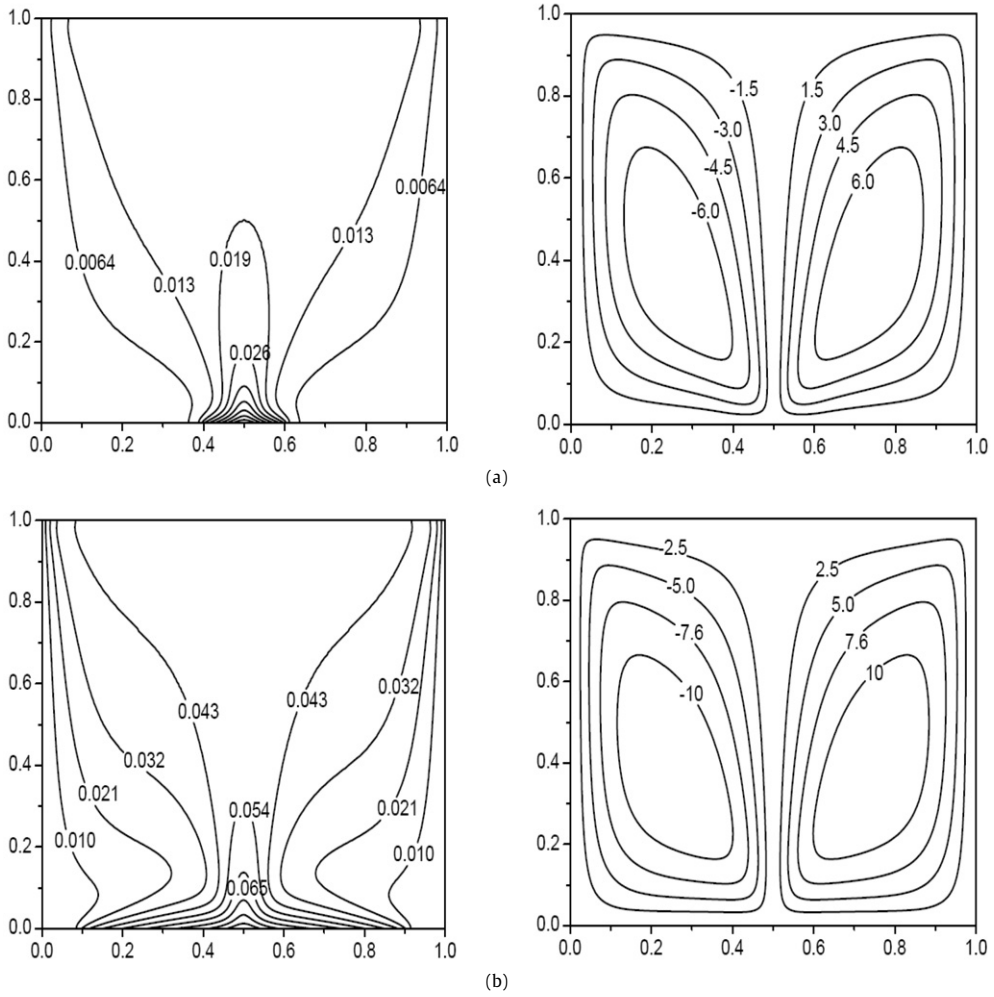

Fig. 12. Isotherms (left) and streamlines (right) with the variation of heat source length for $Ra = 10^8$, $Da = 10^{-4}$, $K^* = 1$, $\theta = 0°$ and $F^* = 1$. (a) $w = 0.2$ ($T_m = 0.0655$); (b) $w = 0.8$ ($T_m = 0.1076$).

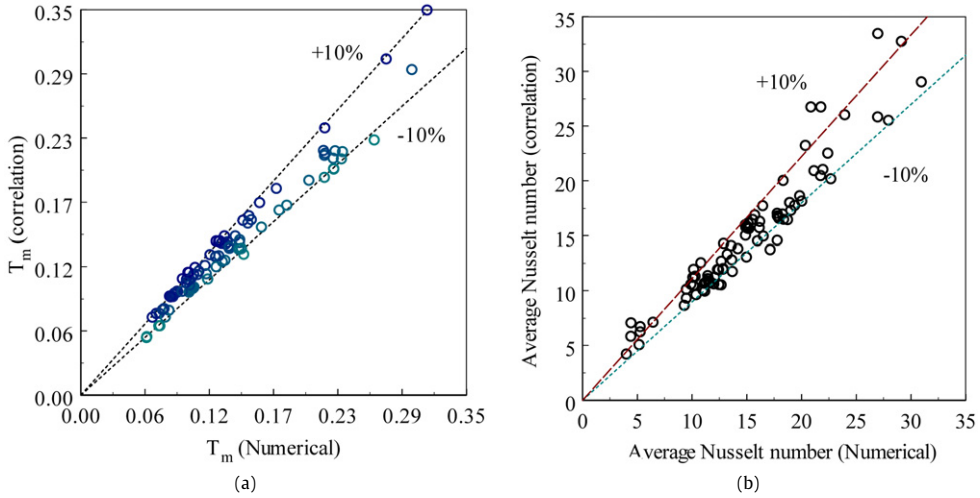

Fig. 13. Parity plot for (a) maximum temperature (T_m), (b) average Nusselt number.

References

[1] J. Ni, C. Beckermann, Natural convection in a vertical enclosure filled with anisotropic porous medium, ASME J. Heat Transfer 113 (1991) 1033–1037.

[2] P. Nithiarasu, K.-S. Sujatha, K. Ravindran, T. Sundararajan, K.-N. Seetharamu, Non-Darcy natural convection in a hydrodynamically and thermally anisotropic porous medium, Computer Methods in Applied Mechanics and Engineering 118 (8) (2000) 413–430.

[3] G. Degan, P. Vasseur, N.-C. Awanou, Anisotropic effects on non-Darcy natural convective from concentrated heat sources in porous media, Acta Mechanica 179 (2005) 111–124.

[4] G. El-Khatib, V. Prasad, Effects of stratification on thermal convection in horizontal porous layers with localized heating from below, ASME J. Heat Transfer 109 (1987) 683–687.

[5] V. Prasad, F.-A. Kulacki, K. Stone, Free convection in a porous cavity with a finite wall heat source, ASME J. Heat Transfer 63 (1986) 91–98.

[6] S.-W. Hsiao, C.-K. Chen, P. Cheng, A numerical solution for natural convection in an inclined porous cavity with discrete heat source on one wall, Int. J. Heat Mass Transfer 37 (15) (1994) 2193–2201.
[7] L. Robillard, C.-H. Wang, V. Vasseur, Multiple steady states in a confined porous medium with localised heating from below, Numerical Heat Transfer 13 (1988) 91–110.
[8] S. Kimura, A. Bejan, Natural convection in a stably heated corner filled with porous medium, ASME J. Heat Transfer 107 (1985) 293–298.
[9] G. Degan, P. Vasseur, E. Bilgen, Convective heat transfer in a vertical anisotropic porous layer, Int. J. Heat Mass Transfer 38 (1995) 1975–1987.
[10] G. Degan, P. Vasseur, Boundary-layer regime in a vertical porous layer with anisotropic permeability and boundary effects, Int. J. Heat Fluid Flow 18 (1) (1997) 334–343.
[11] P. Vasseur, G. Degan, Free convection along a vertical heated plate in a porous medium with anisotropic permeability, Int. J. Numerical Methods for Heat and Fluid Flow 8 (1) (1998) 43–63.
[12] M. Mamou, A. Mahidjiba, P. Vasseur, L. Robillard, Onset of convection in an anisotropic porous medium heated from below by a constant heat flux, Int. Commun. Heat Mass Transfer 25 (6) (1998) 799–808.
[13] J.-L. Lage, Natural convection within a porous medium cavity predicting tools for flow regime and heat transfer, Int. Commun. Heat Mass Transfer 20 (1993) 501–513.
[14] J. Ettefagh, K. Vafai, S.-J. Kim, Non-Darcian effects in open-ended cavities filled with a porous medium, ASME J. Heat Transfer 113 (1991) 747–756.
[15] K. Vafai, C.-L. Tien, Boundary and inertia effects on flow and heat transfer in porous media, Int. J. Heat Mass Transfer 24 (1981) 195–203.
[16] P. Nithiarasu, T. Sundararajan, K.-N. Seetharamu, Natural convective heat transfer in a fluid saturated variable porous medium, Int. J. Heat Mass Transfer 40 (16) (1997) 3955–3967.
[17] A. Nakayama, F. Kuwahara, T. Umemoto, T. Hayashi, Heat and fluid flow within an anisotropic porous medium, ASME J. Heat Transfer 124 (2002) 746–753.
[18] P.-M. Knupp, J.-L. Lage, Generalization of the Forchheimer-extended Darcy flow model to the tensor permeability case via a variational principle, J. Fluid Mechanics 299 (1995) 97–104.
[19] J.-C. Ward, Turbulent flow in porous media, Proc. Amer. Soc. Civil Engg. Journal of Hydraulics Division 90 (5) (1964) 1–12.
[20] D.A. Nield, A. Bejan, Convection in Porous Media, 2nd ed., Springer, New York, 1998.
[21] C. Hirt, A. Amsden, J. Cook, An arbitrary lagrangian eulerian computing method for all flow speeds, Journal of Computational Physics 14 (1974) 227–253.
[22] S.V. Patankar, Numerical Heat Transfer and Fluid Flow, 1st ed., Hemisphere, New York, 1980.
[23] M.A.-R. Sharif, T.R. Mohammad, Natural convective in cavities with constant heat flux heating at the bottom wall and isothermal cooling from the sidewalls, Int. J. Thermal Sciences 44 (2005) 865–878.